Cell Reports

Article

Tuft cells trigger neurogenic inflammation in the urethra

Graphical abstract

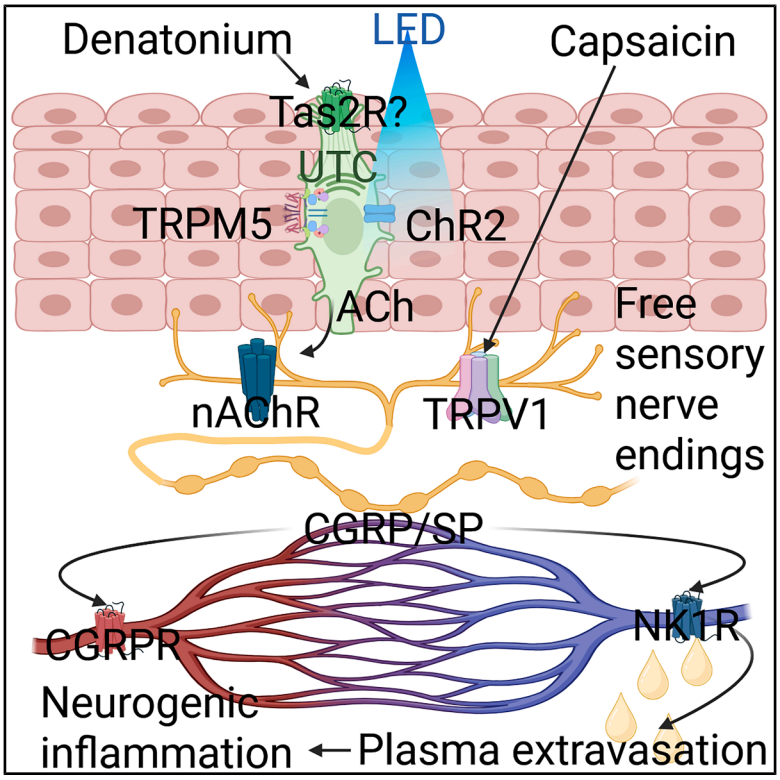

Highlights

- Peptidergic fibers expressing nAChR approach cholinergic urethral tuft cells (UTCs)
- Activation of UTCs triggers acetylcholine (ACh) release
- ACh lead to neuropeptide release from the adjacent nerve terminals
- UTC activation induces neurogenic inflammation, a local defense mechanism

Authors

Patricia Schmidt, Uwe Pfeil, Mahmoud Lafee, ..., Burkhard Schütz, Wolfgang Kummer, Klaus Deckmann

Correspondence

klaus.deckmann@anatomie.med.uni-giessen.de

In brief

Schmidt et al. show that urethral tuft cells (UTCs), which are considered sentinel cells, can trigger neurogenic inflammation by releasing neuropeptides from neighboring nerve fibers, which is regarded as a local defense mechanism.

Schmidt et al., 2025, Cell Reports *44*, 116370
October 28, 2025
https://doi.org/10.1016/j.celrep.2025.116370

CellPress

Cell Reports

CellPress
OPEN ACCESS

Article

Tuft cells trigger neurogenic inflammation in the urethra

Patricia Schmidt,[1,2,6] Uwe Pfeil,[1,2] Mahmoud Lafee,[1,2,3] Swantje Petersen,[1,2] Alexander Perniss,[1,2,7] Maryam Keshavarz,[1,8] Debajyoti Das,[4] Amanda Wyatt,[4] Ulrich Boehm,[4] Burkhard Schütz,[5] Wolfgang Kummer,[1,2] and Klaus Deckmann[1,2,9,10,*]

[1]Institute for Anatomy and Cell Biology, German Center for Lung Research, Justus-Liebig-University Giessen, Gießen, Germany
[2]Excellence Cluster Cardio-pulmonary Institute, Justus-Liebig-University Giessen, Gießen, Germany
[3]Al-Ahliyya Amman University, Amman, Jordan
[4]Department of Pharmacology, Center for Molecular Signaling (PZMS), Center for Gender-Specific Biology and Medicine (CGBM), Saarland University School of Medicine, Homburg, Germany
[5]Institute for Anatomy and Cell Biology, Philipps University, Marburg, Germany
[6]Present address: Leibniz Institute on Aging – Fritz Lipmann Institute, Jena, Germany
[7]Present address: Division of Allergy and Clinical Immunology, Brigham and Women's Hospital and Department of Medicine, Harvard Medical School, Boston, MA, USA
[8]Present address: Anatomy and Cellular Biology, Institute of Theoretical Medicine, Medical Faculty, University of Augsburg, Augsburg, Germany
[9]Senior author
[10]Lead contact
*Correspondence: klaus.deckmann@anatomie.med.uni-giessen.de
https://doi.org/10.1016/j.celrep.2025.116370

SUMMARY

Cholinergic urethral tuft cells (UTCs) are regarded as sentinels of microbial products in the urogenital tract, initiating reflex micturition as a protective mechanism. We here hypothesize that acetylcholine released by stimulated UTC leads to neurogenic inflammation by triggering neuropeptide (substance P and calcitonin gene-related peptide) release from nearby sensory nerve terminals. In the mouse urethra, we find that peptidergic nerve fibers expressing a nicotinic acetylcholine receptor are in contact with UTC. Optogenetic activation of UTC and the UTC activator denatonium leads to the release of neuropeptides from explanted urethrae through cholinergic nicotinic signaling. *In vivo*, intraurethral application of denatonium induces plasma extravasation, a hallmark of neurogenic inflammation, which is sensitive to genetic interruption of the UTC intracellular signaling cascade (Trpm5$^{-/-}$) and blockade of the substance P receptor: neurokinin-1 receptor. Thus, UTCs not only trigger long-distance reflexes involving the bladder but also evoke neurogenic inflammation, representing a local defense reaction.

INTRODUCTION

In the urethra, we previously identified a rare epithelial cell type that produces acetylcholine (ACh) and expresses the canonical taste transduction cascade known from oropharyngeal gustation, including various taste receptors (Tas1r and Tas2r families) and the monovalent cation channel TRPM5 (transient receptor potential cation channel subfamily M member 5). Hence, we named this cell "urethral cholinergic chemosensory cell."[1,2] These cells share several morphologic and functional features with solitary rare cells in the mucosal epithelia of other organs,[3–5] and a common denominator is their developmental dependency on the transcription factor POU class 2 homeobox 3 (Pou2f3).[6] Depending on organ and methods used for their identification, a variety of terms, among them tuft cells referring to an apical tuft of microvilli, has been used for this family.[3] To avoid further confusion, attendants of the first symposium devoted specifically to this cell family, held in August 2023 in Giessen, Germany, reached a consensus to call them tuft cells throughout all organ systems. Accordingly, we here use the term urethral tuft cells (UTCs).

Tuft cells of various proveniences serve as sentinels monitoring the presence of danger-indicating microbial products and metabolites. Once activated, they initiate protective mechanisms through the release of a variety of mediators, including ACh, interleukin-25, cysteinyl-leukotrienes, and prostaglandins.[7] Defense reactions triggered by tuft cells are highly organ-specific and cover a broad spectrum from paracrine signaling to immune,[5,8–11] epithelial,[12–16] and smooth muscle cells[13] to cholinergic excitation of nearby sensory nerve fibers resulting in reflex control of organ function.[1,17,18] These effector mechanisms are not mutually exclusive and can be activated in parallel upon tuft cell stimulation in the small intestine,[11,19] gall bladder,[13] and airways.[12,14]

In the urinary tract, however, our knowledge on tuft cell effector pathways is rather limited. Intraurethral application of the model bitter substance and tuft cell activator denatonium

leads to reflex stimulation of the urinary bladder detrusor muscle, resulting in higher micturition frequency and purging of the urethra, which is considered as a cleaning and, hence, protective mechanism.[1] Locally, sensitivity of UTCs to denatonium is regulated by autocrine cholinergic signaling,[20] but local defense reactions in the urethra have not been reported yet.

We here hypothesized that downstream pathways upon UTC activation are not limited to nervous reflex control of the distant bladder detrusor muscle but also involve local effector mechanisms in the urethra itself. Specifically, we focused upon neurogenic inflammation, since we previously showed that UTCs are able to communicate to sensory neurons by release of ACh,[1] and cholinergic induction of neuropeptide release from certain sensory C-fibers (peptidergic nerve fibers) resulting in neurogenic inflammation is part of the defense repertoire of airway tuft cells.[21–23]

Neurogenic inflammation is a local effector function of nociceptive sensory neurons releasing the neuropeptides substance P (SP) and calcitonin gene-related peptide (CGRP) from their peripheral endings in response to a potentially damaging stimulus. A prototypic stimulus exciting such nerve terminals is capsaicin, an active component of hot chili peppers targeting the cation channel TRPV1 (transient receptor potential cation channel subfamily V member 1),[24,25] but there are also several other triggers known, among them ACh binding to nicotinic ACh receptors (nAChRs).[22,23] Neurogenic inflammation is a compound reaction resulting from the combined action of SP and CGRP. SP is the preferred ligand of the G-protein coupled neurokinin-1 receptor (NK1R) that is expressed by endothelial cells of postcapillary venules. Its activation causes retraction of endothelial cells, leading to the formation of intercellular gaps, through which plasma and with it soluble components of the innate immune defense, leaves the blood stream and leaks into the tissue.[26] CGRP acting on the G-protein-coupled CGRP receptor (CGRPR) is the most potent vasodilator and increases local blood flow. Collectively, this results in acute swelling (plasma extravasation) and redness (vasodilation).[27,28]

On this background, we tested whether UTCs are associated with such peptidergic nerve fibers and whether UTC stimulation triggers SP and CGRP release with subsequent plasma extravasation. Since selective activators of UTCs still have not been identified, we used a previously characterized optogenetic model,[13,15] allowing for direct depolarization of tuft cells in explanted urethrae to study UTC-driven neuropeptide release. Denatonium, a non-selective activator of UTC-driven reflexes upon intraurethral administration,[1] was chosen as chemical stimulus *in vitro* and *in vivo*, where UTCs are not accessible to stimulation with blue light in the optogenetic approach. Since denatonium is not tuft cell-specific but can also activate further cell types,[29] we employed *Trpm5* gene-deficient and UTC-deficient (*Pou2f3*$^{-/-}$) mice to delineate effects dependent on the chemosensory transduction cascade in UTCs from such unspecific reactions.

RESULTS

Peptidergic nerve fibers approach UTCs

A prerequisite of the hypothesized UTC-driven neurogenic inflammation is communication between UTC and peptidergic sensory nerve fibers and, hence, close spatial relationship between them. To elucidate whether UTCs are approached by such fibers, we immunolabeled optically cleared whole urethrae from a UTC reporter mouse line (*Chat*-eGFP) with antibodies against SP and CGRP. Confocal microscopy revealed a dense innervation of the urethra by SP- and CGRP-positive nerve fibers, confirming a previous report[30] (Figure 1A), and eGFP expression driven by the *Chat* promotor was seen both in slender, elongated UTCs and in nerve fibers (Figures 1A and 1B). All classes of fibers traveled in large, longitudinal nerve trunks in the outer, adventitial layer, from which circular bundles, being particularly rich in eGFP- and CGRP-positive fibers, branched toward the muscle layer. Thinner fiber strands in the centrally located mucosa, being particularly rich in SP- and CGRP-positive fibers, were again longitudinally orientated (Figure 1A), showed varicose terminal axons, and gave off fibers penetrating into the epithelium (Figure 1). As previously noted,[30] there was a substantial degree of colocalization of SP- and CGRP immunoreactivities in mucosal sub- and intraepithelial fibers. 42% of the axonal varicosities were double positive for SP and CGRP, with a third of them also exhibiting eGFP expression; 48% were positive for SP but not for CGRP, again with additional eGFP expression in about a third; and only 9% were CGRP^{+} only (Figure S1A). Neurochemical phenotypes of lumbosacral dorsal root ganglia (DRG) neurons matched these observations (Figures S1B and S1C), consistent with a previous report on substantial overlap of *Chat*-eGFP expression and CGRP-immunoreactivity in mouse DRG neurons.[31]

Both SP^{+}/CGRP^{+} and SP^{+}/CGRP^{-} fibers, with and without eGFP expression, approached and made contact with UTCs, as assessed by confocal microscopy (Figures 1B and 1C). Higher magnification revealed nerve fibers in close proximity to and in direct contact with tuft cells, wrapping around the cells (Figures 1D and 1E; see also Videos S1 and S2). In the tracheal epithelium, we recently showed that ACh released from tuft cells does not only act upon immediately neighboring cells but also evokes cholinergic effects some tenths of micrometers away.[14] Therefore, we here considered not only those nerve fibers with direct contact as potential communication partners but also fibers close by and quantified the nearest distance of UTC to peptidergic terminals. Around two-thirds of all UTCs (n = 163; n = 3 urethrae) were closer than 20 μm to the nearest peptidergic nerve fiber (<10 μm: 28%, 10–20 μm: 41%; Figure S2) and, thus, clearly within the tuft cell effector radius known from tuft cells in the tracheal epithelium.[14]

Optogenetic selective activation of UTCs triggers the release of SP

The close spatial relationship between UTCs and peptidergic sensory nerve fibers suggested functional interaction, and we set out to determine whether UTCs can trigger neuropeptide release from such terminals. As a model, we took freshly explanted urethrae, subjected them to UTC stimulation, and measured neuropeptide concentration in the supernatant. Isolated UTCs respond to a variety of chemical stimuli,[1,32,33] but this does not exclude additional effects on other mucosal cell types. Therefore, we used both a chemogenetic and an optogenetic model for direct tuft cell stimulation. In the chemogenetic

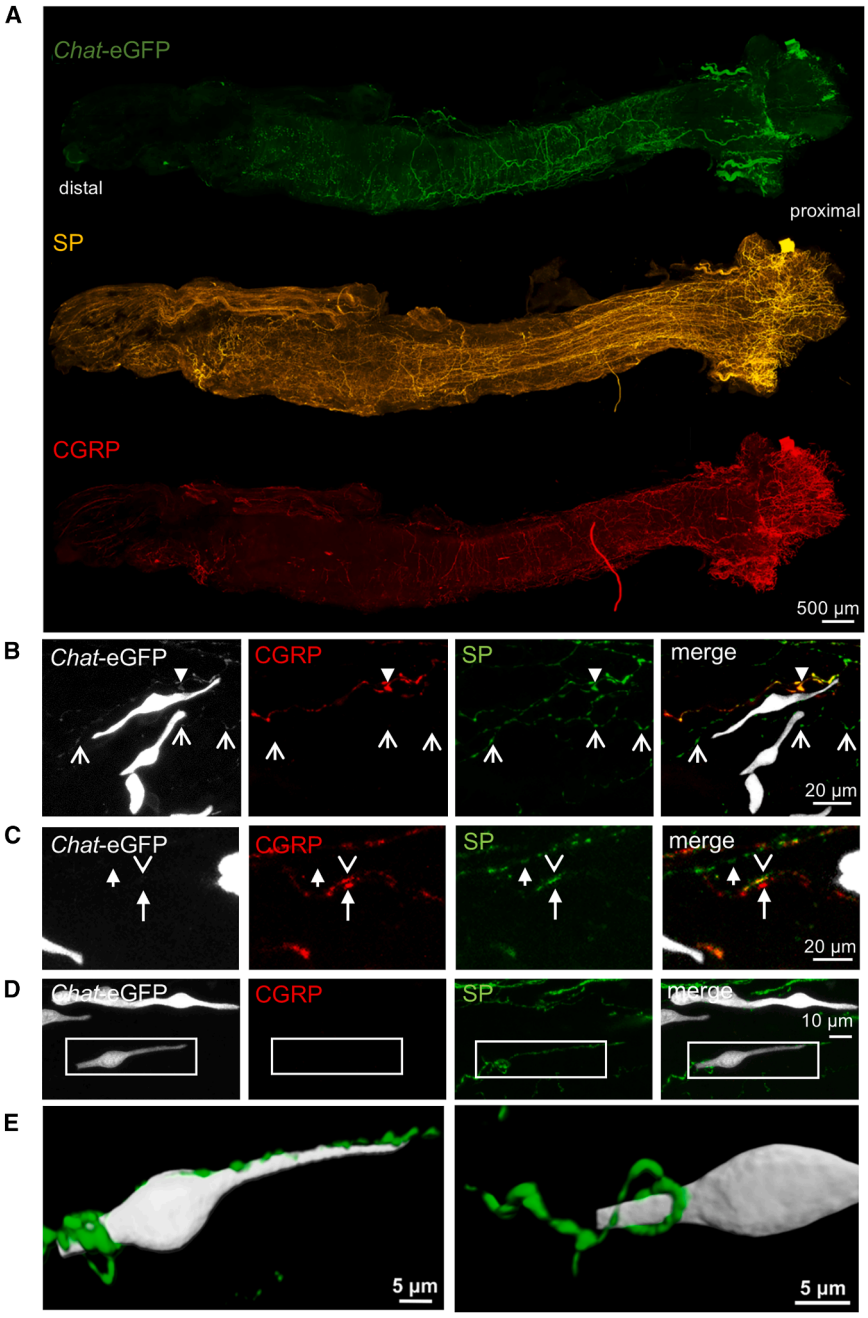

Figure 1. SP and CGRP containing nerve fibers approach UTC

(A) Overview and (B–D) selected magnifications of a cleared urethra from a female *Chat*-eGFP mouse labeled with antibodies against GFP, SP, and CGRP imaged by confocal laser scanning microscopy. UTC appears as elongated *Chat*-eGFP-positive cells. Arrowheads: triple-positive fibers; short arrows: single positive for SP; long arrows: fibers single positive for CGRP; open arrowhead: double positive for SP and CGRP; short open arrows: double positive for SP and GFP.

(E) 3D Reconstruction of a boxed cell in (D) with intimate contacts with an SP-single positive fiber; anterior and posterior view. Scale bar (A) 500 µm, (B and C) 20 µm, (D) 10 µm, and (E) 5 µM. See also Videos S1 and S2.

model (*Trpm5*-DREADD), the *Trpm5* promotor induces the expression of a Gq-coupled DREADD (designer receptor exclusively activated by designer drugs) that can be activated by the synthetic drug clozapine N-oxide (CNO).[34] This strain has been successfully used to evoke ATP release from tuft cells of the mouse trachea by CNO.[35] When applied to isolated urethrae from a conventional wildtype mouse strain (C57BL/6J), CNO was ineffective in our assay but evoked the release of SP into the supernatant to a comparable extent both in *Trpm5*-DREADD and in DREADD control mice (Figure S3); therefore, this model was not suitable for studying our system of interest. This is in line with a previous report on tuft cells in the small intestine, in which a DREADD-based model also proved to be unsuitable to evoke paracrine effects driven by ACh release from tuft cells.[36]

In the optogenetic model, a fusion protein of the blue light-gated cation channel channelrhodopsin-2 (ChR2) and yellow fluorescent protein (YFP) is expressed under the control of the *Chat* promotor (*Chat*-ChR2-YFP).[37] Upon illumination with blue light, ChR2 opens and sodium influx depolarizes the cell.[37] We previously showed that ChR2-YFP is selectively expressed in tuft cells in the trachea and gall bladder in this mouse strain and that blue light from an LED source triggers mediator release from these tuft cells.[13,15] In urethrae of these mice, we observed native YFP fluorescence in the vast majority (88%) of UTCs, identified by immunolabeling for DCLK1 (Figure 2A). DCLK1 is a widely used marker of intestinal tuft cells,[38,39] and immunolabeling of urethral sections from two independent tuft cell reporter mouse strains (*Chat*-eGFP, *Trpm5*-eGFP) confirmed its suitability also for the identification of UTC in both sexes (Figure S4). Importantly, sensory peptidergic fibers in the urethral mucosa did not express *Chat*-ChR2-YFP (Figure S5), excluding direct activation of nerve fibers by blue light in this mouse model.

Explanted *Chat*-ChR2-YFP (ChR2$^+$) and corresponding wild-type (ChR2$^-$) urethrae were stimulated with blue light (456 nm, 10 min, 8 Hz, 25 ms pulse), and supernatants taken before and 10 min after stimulation were analyzed by ELISA for SP content. LED stimulation evoked an increase in SP in the supernatant of *Chat*-ChR2-YFP but not of wild-type urethrae (Figures 2B and S6A), lending support to our hypothesis that UTC stimulation

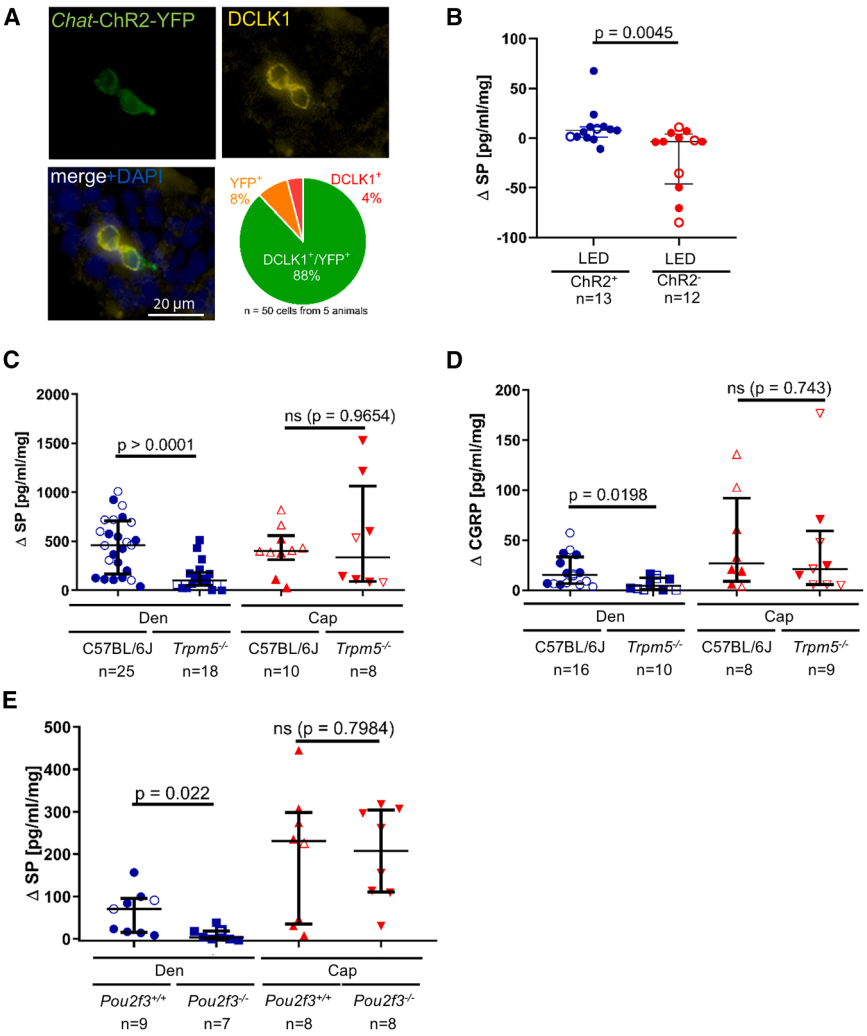

Figure 2. Activation of UTC triggers neuropeptide release

(A) Colocalization of native YFP fluorescence and DCLK1-immunoreactivity (UTC marker) in the urethral epithelium from *Chat*-ChR2-YFP mice; representative fluorescence images and frequencies of phenotypes. Scale bar 20 µm. See also Figures S4 and S5.

(B–E) Increases in the neuropeptide content per mL supernatant related to the weight of the explanted urethra measured by ELISA. (B) Optogenetic model: SP content was determined after a 10-min incubation period with LED of explanted urethrae of *Chat*-ChR2-YFP-positive (ChR2^{+}) and -negative (ChR2^{-}) mice. See also Figure S6A.

(C–E) Chemical stimulation: SP content was determined after the application of denatonium (5 mM) or capsaicin (1 mM) to explanted urethrae from C57BL/6J and Trpm5$^{-/-}$ (C and D) and *Pou2f3*$^{-/-}$ and corresponding wild-type mice (E) mice. See also Figure S11.

(B–E) Δ-values are depicted. Filled symbols: male samples; open symbols: female samples. Whiskers show median and interquartile range; Mann-Whitney test. Data were collected from 4 (B), 16 (C), 17 (D), and 3 (E) independent experiments and analyzed in 8 independent SP-ELISA and 3 independent CGRP-ELISA runs.

can trigger neuropeptide release from sensory nerve terminals, the initial step in neurogenic inflammation.

Denatonium triggers UTC- and TRPM5-dependent release of neuropeptides

This optogenetic model, however, is not suitable for the assessment of real neurogenic inflammation with plasma extravasation in a living organism with functional circulation, because blue light emitted from LED does not penetrate deep enough in the tissue to excite ChR2 expressing UTC *in situ*. Therefore, we searched for a chemical stimulus that mimics the effect seen in the optogenetic experiments *ex vivo* and may then be applied to an *in vivo* setting. We chose the prototypic bitter compound denatonium. Denatonium had been successfully used to activate UTCs upon intraurethral instillation.[1] Exposing urethral explants to denatonium at the concentration used for intraurethral stimulation in the *in vivo* experiments (25 mM)[1] resulted in a very high release of SP from urethrae of both C57BL/6J and *Trpm5*$^{-/-}$ mice (Figure S7). We reasoned that denatonium might directly activate free nerve fibers, which are exposed only in an *in vitro* setup but cannot be reached by an intraurethral stimulation *in vivo* with the intact urothelium forming an effective barrier. Thus, we tested denatonium at three different concentrations (5, 10, and 25 mM) directly on neurons from lumbosacral DRG in calcium imaging. These neurons were isolated from *Chrna3*-eGFP mice, reporting the expression of the ligand-binding α3-subunit of nAChR (nAChRα3; gene name: *Chrna3*). GFP-positive neurons from these ganglia contribute significantly to the sensory innervation of the lower urinary tract.[40] Nicotine application was used to test for their functionality and viability. Among GFP-expressing neurons, responders to denatonium were observed at all tested concentrations (5 mM: 6/19 [33%]; 10 mM: 19/23 [83%]; 25 mM: 12/12 [100%]; Figure S8) and signs of toxicity—loss of GFP fluorescence and of reactivity to subsequent nicotine application—were seen at direct exposure of isolated neurons to 25 mM (Figures S8 and S9).

These neuronal responses to denatonium pointed to the need of using appropriate genetic models or pharmacological intervention to delineate UTC-mediated effects from others when using denatonium as a stimulus. Here, we first used mice deficient for the cation channel TRPM5 (*Trpm5*$^{-/-}$), which is essential for chemosensory signal transduction in tuft cells in general.[13,15,22,23,41] In the urethra, TRPM5 is selectively expressed by UTCs,[1,6] and we here tested whether it might be expressed in lumbosacral DRG. However, neither RT-PCR nor immunofluorescence with TRPM5 antibodies in *Chrna3*-eGFP mice and with GFP antibodies in *Trpm5*-eGFP mice revealed TRPM5 expression in DRG, despite successful positive controls (tongue and

colon; Figure S10). We, therefore, concluded that responses of DRG neurons to denatonium are TRPM5 independent and that TRPM5-dependent reactions are attributable to UTCs.

At 5 mM, denatonium evoked an increase in SP- and CGRP-concentrations in the supernatants of urethrae from C57BL/6J mice. Remarkably, the increase in SP was about 20 times higher than that of CGRP (Figures 2C and 2D), which might be due to the numerous occurrences of $SP^+/CGRP^-$ fibers in addition to those with both peptides (Figure S1A), but SP content might also be higher than that of CGRP when they are colocalized in axons. Stimulated release of both peptides was significantly lower—66% less for SP and 68% less for CGRP—when urethrae were taken from *Trpm5*$^{-/-}$ mice (Figures 2C and 2D), demonstrating dependency on the chemosensory transduction cascade in UTCs. Still, denatonium evoked a residual smaller, but significant release of both peptides from the urethrae of *Trpm5*$^{-/-}$ mice (Figures 2C, 2D, S10A-B), indicating a contribution of unspecific, TRPM5-independent direct effects on sensory fibers.

These findings were fully corroborated using UTC-deficient mice as a second model. The transcription factor Pou2f3 is essential for the development of tuft cells, and *Pou2f3*$^{-/-}$ mice are generally devoid of tuft cells, including UTCs.[6] Similar as in Trpm5$^{-/-}$ mice, denatonium (5 mM) evoked a significantly lower release of SP from the urethrae of *Pou2f3*$^{-/-}$ mice compared to wild-type littermates (Figures 2E and S11C).

Capsaicin triggered a UTC-independent release of SP and CGRP (Figures 2C–2E; Figure S11), consistent with its known direct effect on TRPV1-positive peptidergic nerve fibers.

Collectively, these data showed that denatonium is a stimulus inducing a UTC-dependent neuropeptide release from urethral sensory fibers through a pathway involving TRPM5 signaling in UTC.

Nicotinic receptors drive neuropeptide release induced by UTCs

All hitherto known examples of tuft cell-to-neuron communication rely on cholinergic signaling with tuft cell-derived ACh acting upon ACh receptors on sensory nerve fibers,[1,18,22,23] and in cases in which a pharmacological discrimination between muscarinic and nicotinic signaling has been achieved, this operates through nAChR.[1,18,22] The dominant, although not the sole, ligand-binding nAChR subunit expressed by sensory neurons is the α3 subunit (gene name: *Chrna3*),[42,43] and we previously showed that nerve fibers expressing this subunit establish contact to UTCs.[1] We now asked whether the peptidergic fibers identified in the present study represent a separate entity or express *Chrna3*, which would make them responsive to UTC-derived ACh.

We addressed this question in immunolabeled cleared whole urethrae, utilizing a *Chrna3* reporter mouse strain (*Chrna3*-eGFP) and antibodies against one of the neuropeptides (SP and CGRP) and against DCLK1 as a tuft cell marker. Three neurochemical phenotypes of nerve fibers were found next to $DCLK1^+$ UTC: 1) peptidergic (SP^+ or $CGRP^+$) fibers also expressing *Chrna3*-driven eGFP (further on designated $nAChR\alpha3^+$), 2) peptidergic fibers without eGFP expression, and 3) $nAChR\alpha3^+$ fibers without peptide-immunoreactivity (Figures 3A and 3B). The same phenotypes were observed when a TRPM5 antibody was used as an UTC marker and immunolabeling was done on tissue sections (Figure S12). Double-positive axonal varicosities (SP^+ or $CGRP^+/nAChR\alpha3^+$) made up 12–16% of the labeled population, purely peptidergic (SP^+ or $CGRP^+$) fibers around 40%, and non-peptidergic $nAChR\alpha3^+$ fibers about 45–50% (Figure S12).

These data showed neurochemical heterogeneity of nerve fibers approaching UTCs, including a phenotype that is suited to release neuropeptides upon cholinergic activation of nAChR. To address this possibility directly, we tested the effects of a general nAChR antagonist (mecamylamine, 20 μM) on SP release upon the stimulation of UTC in the explanted urethra preparation. Consistent with our hypothesis, mecamylamine completely inhibited SP release induced by LED illumination in the optogenetic model (Figures 3C and S6B), and it significantly reduced the increase when denatonium was used as a stimulus. In contrast, a general muscarinic AChR antagonist (atropine, 2 μM) was ineffective in reducing SP release when denatonium was used as a stimulus (Figures 4D and S6C).

Denatonium induces TRPM5-dependent neurogenic plasma extravasation in the urethra

The data so far established that TRPM5-dependent activation of UTC leads to nAChR-dependent neuropeptide release from sensory nerve fibers *in vitro* in explanted urethrae. We next tested whether this chain of events finally leads to neurogenic inflammation *in vivo* by instillation of test substances (denatonium, capsaicin, and PBS) into the urethra in anesthetized animals. Given the dilution effect that occurs upon instillation, and the especially tight barrier formed by the epithelium of the lower urinary tract,[44–46] higher concentrations than usually taken for experiments on isolated cells were used (denatonium 25 mM, capsaicin 10 mM). Intraurethral application of denatonium led to significantly increased plasma extravasation recorded photometrically in the urethrae of C57BL/6J mice, with only a tendency toward increase ($p = 0.051$) in the bladder (Figures 4A and S13A). This effect was critically dependent on TRPM5, as it was not observed in *Trpm5*$^{-/-}$ mice (Figures 4A and S13A). Capsaicin, a direct activator of peptidergic sensory nerve fibers through its action upon TRPV1, evoked plasma extravasation exceeding that induced by denatonium in the urethra and bladder of both C57BL/6J and *Trpm5*$^{-/-}$ mice upon instillation into the urethra (Figures 4A and S13A).

To validate these findings by an independent technique, Evans blue plasma extravasation was assessed by fluorescence microscopy of urethral tissue sections. Histological evaluation of urethrae stimulated with denatonium showed a significant increase in fluorescence intensity in the urethral epithelium of C57BL/6J mice, when compared to the control group. Again, this effect was TRPM5 dependent and not seen in *Trpm5*$^{-/-}$ mice (Figures 4B and 4C). Capsaicin evoked an increase in epithelial fluorescence intensity independent of TRPM5 (Figures 4B and 4C), consistent with its known direct effect upon TRPV1-positive peptidergic nerve terminals. Collectively, these data demonstrated that denatonium induces plasma extravasation in the urethra through a signaling pathway involving TRPM5, which is selectively expressed in UTCs in this organ.

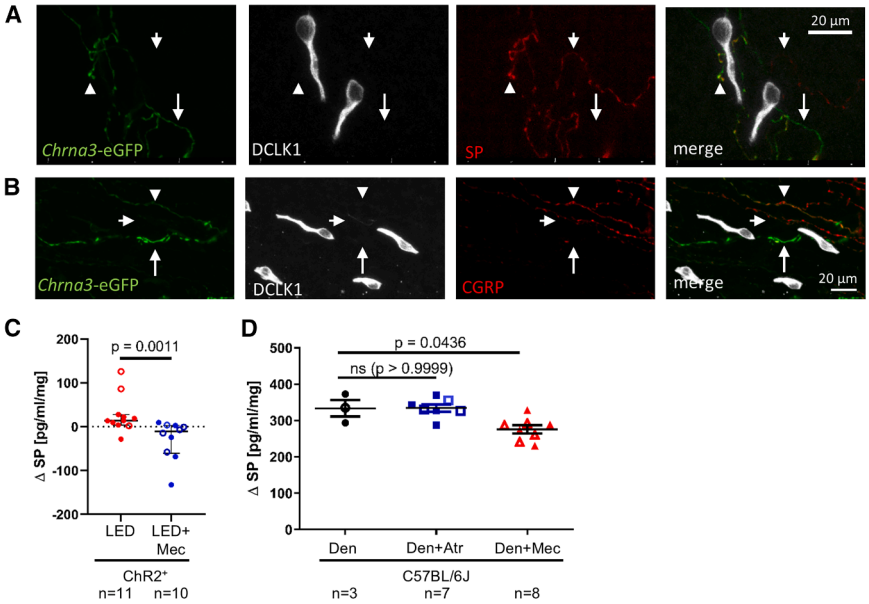

Figure 3. Peptidergic nerve fibers approaching UTC are cholinoceptive

(A and B) Cleared female urethrae from *Chrna3*-eGFP mice (n = 3) labeled with antibodies against GFP, DCLK1 (UTC marker), and (A) SP or (B) CGRP. Arrowheads: GFP/neuropeptide double-positive fibers; short arrows: fibers single positive for SP or CGRP. Long arrows: fibers single positive for GFP. Scale bar 20 µm. See also Figure S12.

(C and D) Increases in SP content per mL supernatant related to the weight of the explanted urethra measured by ELISA. (C) Optogenetic model: SP content was first determined after 10-min incubation of urethrae from *Chat*-ChR2-YFP$^+$ mice without LED and then after a 10-min incubation period with LED in the presence or absence of mecamylamine (Mec; 20 µM); Δ-values are depicted. See also Figure S6B. (D) Increases in SP content in urethral supernatants in response to stimulation (10 min) with denatonium (Den, 5 mM), denatonium plus atropine (Den, 5 mM, + Atr, 2 µM), or denatonium plus mecamylamine (Den, 5 mM + Mec, 20 µM) in C57BL/6J mice. See also Figure S6C.

Whiskers show median and interquartile range; (C) Mann-Whitney test. (D) Kruskal-Wallis test followed by post hoc Dunn's multiple comparison test. Data were collected from 4 (C) or 3 (D) independent experiments.

UTC-mediated plasma extravasation is dependent on nicotinic and NK1Rs

Our working model of neurogenic inflammation driven by UTCs postulates cholinergic transmission from UTCs to nAChRs on sensory nerve fibers and subsequent release of SP acting upon NK1Rs on endothelial cells. Accordingly, the general nAChR antagonist mecamylamine significantly reduced plasma extravasation in the urethra evoked by denatonium, whereas atropine did not (Figure 4A). Effects in the urinary bladder were not seen (Figure S13A). Among the inhibitors of neuropeptide receptors, CP96345, a potent and selective NK1R antagonist, significantly reduced Evans blue plasma extravasation in response to denatonium, whereas a trend toward a reduction caused by BIBN4096BS, a CGRPR antagonist, did not reach significance (Figure 4A). Both inhibitors were also effective in lowering plasma extravasation evoked by capsaicin, demonstrating that they acted downstream to nerve fiber stimulation (Figure S13B).

DISCUSSION

This study demonstrates a complex association of UTC with several neurochemically distinct types of sensory nerve fibers and establishes neurogenic inflammation as a local defense mechanism triggered by the stimulation of UTCs, in addition to the previously reported facilitation of bladder detrusor activity.[1] Mechanistically, we here identified nicotinic cholinergic transmission as the communication route from UTCs to sensory nerve fibers, resulting in peptide release and neurogenic inflammation, similar to what has been described for the airways.[21–23] The presence of a substantial number of nAChRα3-negative peptidergic fibers in the vicinity of UTCs may suggest that further, non-nicotinic pathways may operate in parallel, which would offer an explanation for the observation that the general nicotinic blocker mecamylamine significantly reduced, but by far not abolished SP release induced by denatonium application onto the explanted urethra. On the other hand, denatonium showed some direct, unspecific effects on isolated sensory neurons, and mecamylamine fully abrogated SP release upon selective optogenetic activation of UTC, strongly arguing for an exclusive role of cholinergic transmission and nAChR. This might also involve nAChRα3-negative peptidergic fibers, since we previously showed that sensory neurons projecting to the mouse lower urinary tract can express nAChR with other α-subunits than α3, in particular α6 and α7.[40]

The downstream mechanisms followed the known general principles of neurogenic inflammation evoked by the activation of peptidergic nociceptor fibers in many other organs,[22,23,27,28,47,48] including the release of SP and CGRP with plasma extravasation primarily driven by SP acting upon NK1R. Specifically in the urethra, it can be triggered by mechanical stimulation (catheterization),[49] direct antidromic electrical nerve stimulation, and application of capsaicin, an activator of the TRPV1 channel being characteristic for nociceptors.[50–52] Thus, it is not a program uniquely driven by UTCs. Rather, UTCs channel their response into a general innate defense program and serve as a relay extending the spectrum of triggers to stimuli to which peptidergic terminals are not sensitive on their own. Despite the similarities between the responses to capsaicin and to UTC stimulation, they are not necessarily conveyed by one and the same population of nerve fibers. For example, neurogenic inflammation in response to mechanical irritation of the urethral mucosa (catheterization) is mediated to about equal extent both by capsaicin-sensitive and -insensitive fibers.[49] The

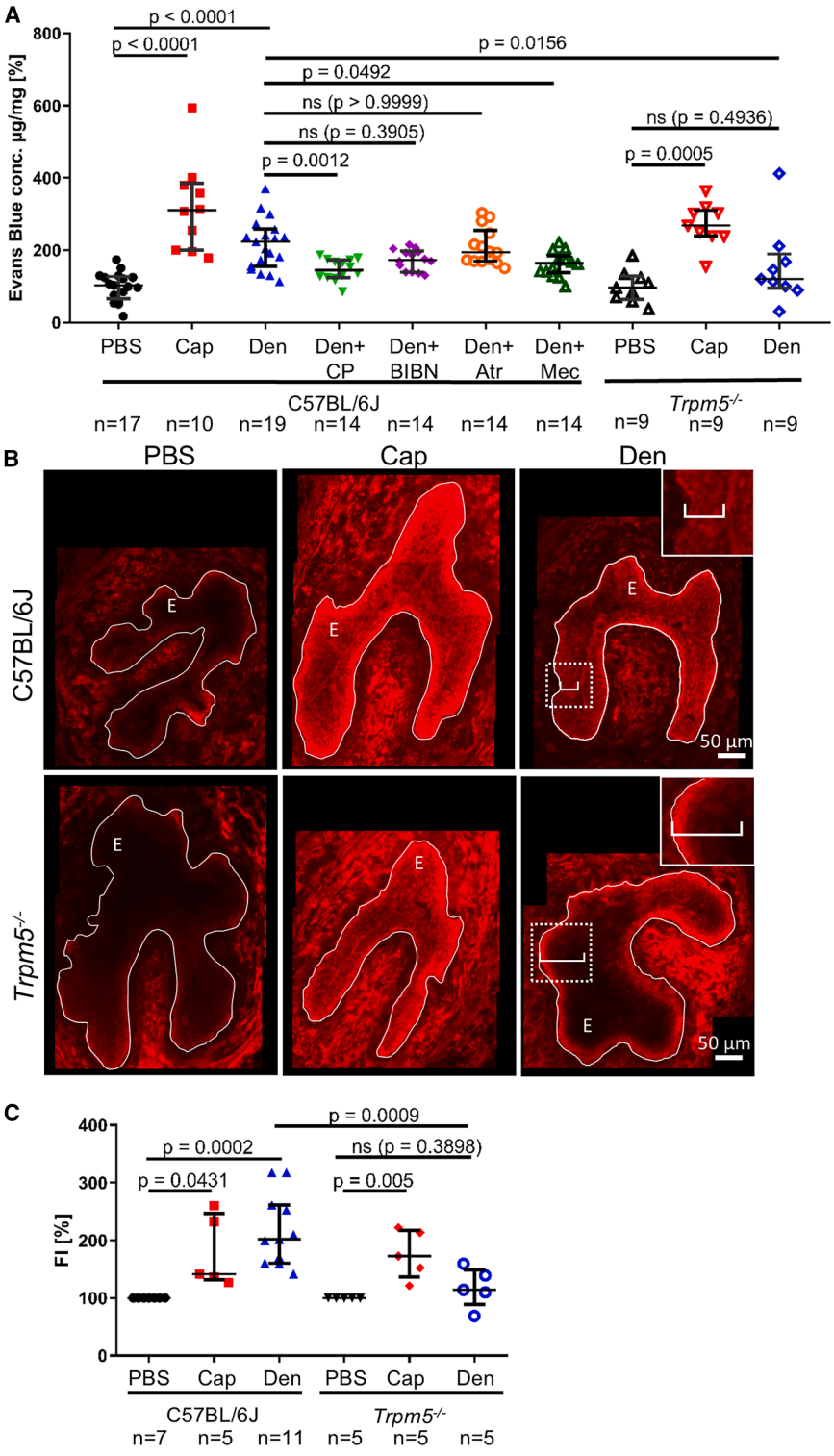

Figure 4. Denatonium triggers TRPM5-dependent plasma extravasation

(A) Photometric assessment of Evans blue concentration per mg tissue as readout of plasma extravasation in urethrae of female C57BL/6J and *Trpm5*$^{-/-}$ mice after the intraurethral application of PBS, capsaicin (Cap, 10 mM), or denatonium (Den, 25 mM) for 15 min after the intravenous injection of Evans blue. The neuropeptide receptor antagonists CP96345 (CP, NK1R antagonist, 10 mg/kg) and BIBN4096BS (BIBN, CGRPR antagonist, 1 mg/kg) were given intravenously together with Evans blue, and the cholinergic receptor blockers atropine (Atr, 10 µM) and mecamylamine (Mec, 20 µM) were applied into the urethra together with denatonium. Evans blue concentration is given in percent related to the PBS control. Whiskers show median and interquartile range. Kruskal-Wallis test followed by post hoc Dunn's multiple comparison test for analyses of multiple groups within one strain; Mann-Whitney test for two-group comparison of the denatonium response in two strains. Data were collected from 27 independent experiments.

(B) Fluorescence microscopical demonstration of the red fluorescence emitted by Evans blue when excited with green light (525–560 nm) in 10-µm thick urethral cross sections of female C57BL/6J and *Trpm5*$^{-/-}$ mice after the intraurethral application of PBS, capsaicin (Cap, 10 mM), or denatonium (Den, 25 mM) for 15 min. All images were taken at identical magnification (20× objective lens) and exposure time (30 ms). Insets show higher magnification of boxed areas. Height of the epithelial layer (E) indicated by brackets; white line marks the basal membrane and thus the boundary between the epithelial layer and the lamina propria. Scale bar 50 µm.

(C) Fluorescence intensity of epithelial layer evaluated using ImageJ and shown relative to PBS control and per mm^2 urethral epithelium. Each data point represents the mean fluorescence intensity from at least 10 sections per animal taken at least 100 µm apart. Whiskers show median and interquartile range. Kruskal-Wallis test followed by post hoc Dunn's multiple comparison test for analyses of multiple groups within one strain; Mann-Whitney test for two-group comparison of the denatonium response in two strains. Data were collected from 12 independent experiments.

phenotypic diversity of peptidergic fibers connected to UTCs suggests that here also, more than one type of nerve fibers may be involved, and their capsaicin sensitivity remains to be clarified.

Neurogenic inflammation extends beyond initial, acute vascular effects and includes the activation of resident immune cells such as mast cells and recruitment of leukocytes from the blood stream, as it has also been shown after tuft cell activation in the mouse nasal cavity (also called solitary chemosensory cells at this site) and trachea.[22,23] In the urethra, such effects on immune cells have been directly investigated neither by us nor in previous studies on neurogenic inflammation,[49,50,52] but given the stereotypic character of this program, they are likely

to occur in the urethra as well. Plasma extravasation, the early hallmark on which we had set our focus, has at least two consequences. First, circulating soluble factors of the immune system can enter the tissue and may act as a first line of defense.[23,53] Second, the resulting edema causes local swelling, which may also serve a defense function due to mechanical effects, as has been shown in the vomeronasal duct opening into the nose. There, neurogenic inflammation initiated by the activation of tuft cells results in the obstruction of the vomeronasal duct, thereby limiting access of potentially harmful substances to the cavity of the vomeronasal organ.[21] In the urinary tract, ascent of bacteria through the urethra is an important route of acquiring infection,[54–57] and swelling resulting from UTC-induced neurogenic inflammation might hinder further progress toward the bladder and deeper into the urinary tract.

In terms of protection against infection, such a denial-of-ingress mechanism can be considered a meaningful synergism to the previously identified expulsion mechanism represented by reflex facilitation of detrusor activity and micturition.[1] At first sight, initiation of a neurogenic inflammation in the urethra together with enhanced reflex bladder contraction appears unexpected, because intraurethral application of capsaicin, which causes plasma extravasation in the urethra,[50,51] is generally reported to suppress rather than enhance reflex bladder contractions.[58–60] However, the reflex response to intraurethral capsaicin is biphasic, with an initial increase in bladder contraction frequency, which then diminishes and turns into inhibition in the next 15–30 min. This delayed inhibition has been interpreted as the consequence of the known marked desensitizing effect of capsaicin on TRPV1-carrying sensory fibers, so that the initial increase in detrusor activity remains as the reflex response of acute stimulation[61] matching what happens after UTC activation. It also has to be considered that, although both neural responses induced by UTCs, i.e., neurogenic inflammation and reflex facilitation, rely on nicotinic cholinergic communication from UTCs to sensory nerve fibers, they could be mediated by distinct sets of nerve fibers. Indeed, the marked neurochemical diversity of sensory nerve fibers next to UTCs argues for the involvement of more than one fiber type. Among them, the non-peptidergic nAChR$\alpha3^+$ fibers are equipped to generate a nicotinic response to ACh without concomitant SP release and plasma extravasation and, thus, are candidates for triggering bladder reflexes independently. Given the multiplicity of neurochemical phenotypes of sensory fibers approaching UTCs, it does not appear to be unlikely that additional neural pathways linked to UTC stimulation still await to be unraveled.

Limitations of the study

A clear limitation of this and earlier studies of UTCs is that we still have not identified a selective activator. UTC are polymodal sensors and respond to a broad spectrum of substances, such as bitter compounds, sugars, ATP, glutamate, and high salt, but all of them can also activate other cells in the urethra.[1,32,33] Thus, *in vivo* studies using broadly acting stimulants such as the widely employed bitter tastant denatonium will result in mixed reactions, consisting of UTC-dependent and UTC-independent responses, which then need to be dissected by appropriate pharmacological interventions and genetic models. Blockade of cholinergic transmission, genetic deletion of *Trpm5*, and the use of mice lacking UTC (*Pou2f3*$^{-/-}$) were approaches in that direction that we used in this study, but of course, they also have their own limitations. At least for those experiments, which can be conducted *ex vivo* with explanted urethrae, we here could overcome this limitation by establishing an optogenetic model for the study of UTCs, which unequivocally demonstrated the link between activated UTCs and neuropeptide release from sensory nerve fibers through cholinergic nicotinic transmission. This approach also clearly unmasked the extent of UTC-independent effects when using a non-selective activator, as the nicotinic blocker mecamylamine entirely abrogated SP release in the optogenetic experiment, whereas more than 50% remained when denatonium was used as a stimulus. Still, although optogenetics solved the problems for the current set of experiments on explanted urethras, this approach has also limitations in that it 1) is barely applicable to the urethra *in vivo*, and 2) triggers only such UTC reactions that are dependent on sodium influx/depolarization. Thus, a selective UTC activator is still warranted for future studies.

RESOURCE AVAILABILITY

Lead contact

Further information and requests for resources and reagents should be directed to and will be fulfilled by the lead contact, Klaus Deckmann (klaus.deckmann@anatomie.med.uni-giessen.de).

Materials availability

This study did not generate unique reagent.

Data and code availability

- All data reported in this paper will be shared by the lead contact upon request.
- This paper does not report original code.
- Any additional information required to re-analyze the data reported in this paper is available from the lead contact upon request.

ACKNOWLEDGMENTS

We thank Martin Bodenbenner, Silke Wiegand, Petra Mermer, and Tamara Papadakis for technical assistance. We thank Vladimir Chubanov and Thomas Gudermann, Ludwig-Maximilian-University Munich, for providing TRPM5 antibody. We also thank Astrid Weiβ, Justus-Liebig-University Giessen, Germany, for technical support in ELISA data analysis and Praju Vikas Anekal from MicRoN (Microscopy Resources on the North Quad) Core, Harvard Medical School, Boston, USA, for helping with 3D rendering. We gratefully acknowledge the Micron Core for giving us access to the Arivis Vision4D software. This work was supported by a University Hospital Giessen and Marburg (UKGM)-Justus-Liebig-University (JLU)-Cooperation Grant (# 7/2016 GI to K.D.), the Excellence Cluster Cardio-Pulmonary Institute (CPI, EXC 147 to W.K.), the Else Kröner-Fresenius-Stiftung (2016_A90 to K.D.), the German Research Foundation (DFG, 544054869 to K.D.), and a scholarship from Al-Ahliyya Amman University (PO/1/35/3216 to M.L.).

AUTHOR CONTRIBUTIONS

K.D., W.K., and P.S. designed the research and performed statistical analysis. K.D., P.S., U.P., A.P., M.K., M.L., S.P., B.S., D.D., A.W., U.B., and W.K. performed the research and analyzed data. K.D. and W.K. obtained funding. K. D., P.S., and W.K. drafted the manuscript. This work was supervised by K. D., U.B., and W.K.

DECLARATION OF INTERESTS

The authors declare no competing interests.

STAR★METHODS

Detailed methods are provided in the online version of this paper and include the following:

- KEY RESOURCES TABLE
- EXPERIMENTAL MODEL AND STUDY PARTICIPANT DETAILS
  - Animals
- METHOD DETAILS
  - Immunofluorescence
  - Assessment of neuropeptide release from explanted urethrae
  - Calcium imaging
  - RT-PCR
  - Plasma extravasation
- QUANTIFICATION AND STATISTICAL ANALYSIS

SUPPLEMENTAL INFORMATION

Supplemental information can be found online at https://doi.org/10.1016/j.celrep.2025.116370.

Received: January 10, 2025
Revised: July 4, 2025
Accepted: September 13, 2025

REFERENCES

1. Deckmann, K., Filipski, K., Krasteva-Christ, G., Fronius, M., Althaus, M., Rafiq, A., Papadakis, T., Renno, L., Jurastow, I., Wessels, L., et al. (2014). Bitter triggers acetylcholine release from polymodal urethral chemosensory cells and bladder reflexes. Proc. Natl. Acad. Sci. USA *111*, 8287–8292. https://doi.org/10.1073/pnas.1402436111.
2. Deckmann, K., Krasteva-Christ, G., Rafiq, A., Herden, C., Wichmann, J., Knauf, S., Nassenstein, C., Grevelding, C.G., Dorresteijn, A., Chubanov, V., et al. (2015). Cholinergic urethral brush cells are widespread throughout placental mammals. Int. Immunopharmacol. *29*, 51–56. https://doi.org/10.1016/j.intimp.2015.05.038.
3. Pan, J., Zhang, L., Shao, X., and Huang, J. (2020). Acetylcholine From Tuft Cells: The Updated Insights Beyond Its Immune and Chemosensory Functions. Front. Cell Dev. Biol. *8*, 606. https://doi.org/10.3389/fcell.2020.00606.
4. Strine, M.S., and Wilen, C.B. (2022). Tuft cells are key mediators of interkingdom interactions at mucosal barrier surfaces. PLoS Pathog. *18*, e1010318. https://doi.org/10.1371/journal.ppat.1010318.
5. O'Leary, C.E., Schneider, C., and Locksley, R.M. (2019). Tuft Cells-Systemically Dispersed Sensory Epithelia Integrating Immune and Neural Circuitry. Annu. Rev. Immunol. *37*, 47–72. https://doi.org/10.1146/annurev-immunol-042718-041505.
6. Yamashita, J., Ohmoto, M., Yamaguchi, T., Matsumoto, I., and Hirota, J. (2017). Skn-1a/Pou2f3 functions as a master regulator to generate Trpm5-expressing chemosensory cells in mice. PLoS One *12*, e0189340. https://doi.org/10.1371/journal.pone.0189340.
7. Kotas, M.E., O'Leary, C.E., and Locksley, R.M. (2023). Tuft Cells: Context- and Tissue-Specific Programming for a Conserved Cell Lineage. Annu. Rev. Pathol. *18*, 311–335. https://doi.org/10.1146/annurev-pathol-042320-112212.
8. Bankova, L.G., Dwyer, D.F., Yoshimoto, E., Ualiyeva, S., McGinty, J.W., Raff, H., von Moltke, J., Kanaoka, Y., Frank Austen, K., and Barrett, N.A. (2018). The cysteinyl leukotriene 3 receptor regulates expansion of IL-25-producing airway brush cells leading to type 2 inflammation. Sci. Immunol. *3*, eaat9453. https://doi.org/10.1126/sciimmunol.aat9453.
9. Bornstein, C., Nevo, S., Giladi, A., Kadouri, N., Pouzolles, M., Gerbe, F., David, E., Machado, A., Chuprin, A., Tóth, B., et al. (2018). Single-cell mapping of the thymic stroma identifies IL-25-producing tuft epithelial cells. Nature *559*, 622–626. https://doi.org/10.1038/s41586-018-0346-1.
10. Gerbe, F., Sidot, E., Smyth, D.J., Ohmoto, M., Matsumoto, I., Dardalhon, V., Cesses, P., Garnier, L., Pouzolles, M., Brulin, B., et al. (2016). Intestinal epithelial tuft cells initiate type 2 mucosal immunity to helminth parasites. Nature *529*, 226–230. https://doi.org/10.1038/nature16527.
11. von Moltke, J., Ji, M., Liang, H.E., and Locksley, R.M. (2016). Tuft-cell-derived IL-25 regulates an intestinal ILC2-epithelial response circuit. Nature *529*, 221–225. https://doi.org/10.1038/nature16161.
12. Hollenhorst, M.I., Jurastow, I., Nandigama, R., Appenzeller, S., Li, L., Vogel, J., Wiederhold, S., Althaus, M., Empting, M., Altmüller, J., et al. (2020). Tracheal brush cells release acetylcholine in response to bitter tastants for paracrine and autocrine signaling. FASEB J. *34*, 316–332. https://doi.org/10.1096/fj.201901314RR.
13. Keshavarz, M., Faraj Tabrizi, S., Ruppert, A.L., Pfeil, U., Schreiber, Y., Klein, J., Brandenburger, I., Lochnit, G., Bhushan, S., Perniss, A., et al. (2022). Cysteinyl leukotrienes and acetylcholine are biliary tuft cell cotransmitters. Sci. Immunol. *7*, eabf6734. https://doi.org/10.1126/sciimmunol.abf6734.
14. Perniss, A., Boonen, B., Tonack, S., Thiel, M., Poharkar, K., Alnouri, M.W., Keshavarz, M., Papadakis, T., Wiegand, S., Pfeil, U., et al. (2023). A succinate/SUCNR1-brush cell defense program in the tracheal epithelium. Sci. Adv. *9*, eadg8842. https://doi.org/10.1126/sciadv.adg8842.
15. Perniss, A., Liu, S., Boonen, B., Keshavarz, M., Ruppert, A.L., Timm, T., Pfeil, U., Soultanova, A., Kusumakshi, S., Delventhal, L., et al. (2020). Chemosensory Cell-Derived Acetylcholine Drives Tracheal Mucociliary Clearance in Response to Virulence-Associated Formyl Peptides. Immunity *52*, 683–699.e11. https://doi.org/10.1016/j.immuni.2020.03.005.
16. Billipp, T.E., Fung, C., Webeck, L.M., Sargent, D.B., Gologorsky, M.B., McDaniel, M.M., Kasal, D.N., McGinty, J.W., Barrow, K.A., Rich, L.M., et al. (2023). Tuft cell-derived acetylcholine regulates epithelial fluid secretion. Preprint at bioRxiv, 2023.03.17.533208. https://doi.org/10.1101/2023.03.17.533208.
17. Tizzano, M., Gulbransen, B.D., Vandenbeuch, A., Clapp, T.R., Herman, J.P., Sibhatu, H.M., Churchill, M.E.A., Silver, W.L., Kinnamon, S.C., and Finger, T.E. (2010). Nasal chemosensory cells use bitter taste signaling to detect irritants and bacterial signals. Proc. Natl. Acad. Sci. USA *107*, 3210–3215. https://doi.org/10.1073/pnas.0911934107.
18. Krasteva, G., Canning, B.J., Hartmann, P., Veres, T.Z., Papadakis, T., Mühlfeld, C., Schliecker, K., Tallini, Y.N., Braun, A., Hackstein, H., et al. (2011). Cholinergic chemosensory cells in the trachea regulate breathing. Proc. Natl. Acad. Sci. USA *108*, 9478. https://doi.org/10.1073/pnas.1019418108.
19. Schneider, C., O'Leary, C.E., Von Moltke, J., Liang, H.-E., Ang, Q.Y., Turnbaugh, P.J., Radhakrishnan, S., Pellizzon, M., Ma, A., and Locksley, R.M. (2018). A Metabolite-Triggered Tuft Cell-ILC2 Circuit Drives Small Intestinal Remodeling. Cell *174*, 271–284.e14. https://doi.org/10.1016/j.cell.2018.05.014.
20. Deckmann, K., Rafiq, A., Erdmann, C., Illig, C., Durschnabel, M., Wess, J., Weidner, W., Bschleipfer, T., and Kummer, W. (2018). Muscarinic receptors 2 and 5 regulate bitter response of urethral brush cells via negative feedback. FASEB J. *32*, 2903–2910. https://doi.org/10.1096/fj.201700582R.
21. Ogura, T., Krosnowski, K., Zhang, L., Bekkerman, M., and Lin, W. (2010). Chemoreception regulates chemical access to mouse vomeronasal organ: role of solitary chemosensory cells. PLoS One *5*, e11924. https://doi.org/10.1371/journal.pone.0011924.
22. Saunders, C.J., Christensen, M., Finger, T.E., and Tizzano, M. (2014). Cholinergic neurotransmission links solitary chemosensory cells to nasal

inflammation. Proc. Natl. Acad. Sci. USA *111*, 6075–6080. https://doi.org/10.1073/pnas.1402251111.

23. Hollenhorst, M.I., Nandigama, R., Evers, S.B., Gamayun, I., Abdel Wadood, N., Salah, A., Pieper, M., Wyatt, A., Stukalov, A., Gebhardt, A., et al. (2022). Bitter taste signaling in tracheal epithelial brush cells elicits innate immune responses to bacterial infection. J. Clin. Investig. *132*, e150951. https://doi.org/10.1172/JCI150951.
24. Basbaum, A.I., Bautista, D.M., Scherrer, G., and Julius, D. (2009). Cellular and molecular mechanisms of pain. Cell *139*, 267–284. https://doi.org/10.1016/j.cell.2009.09.028.
25. Julius, D. (2013). TRP channels and pain. Annu. Rev. Cell Dev. Biol. *29*, 355–384. https://doi.org/10.1146/annurev-cellbio-101011-155833.
26. Baluk, P., Thurston, G., Murphy, T.J., Bunnett, N.W., and McDonald, D.M. (1999). Neurogenic plasma leakage in mouse airways. Br. J. Pharmacol. *126*, 522–528. https://doi.org/10.1038/sj.bjp.0702323.
27. Holzer, P. (1992). Peptidergic sensory neurons in the control of vascular functions: mechanisms and significance in the cutaneous and splanchnic vascular beds. Rev. Physiol. Biochem. Pharmacol. *121*, 49–146. https://doi.org/10.1007/BFb0033194.
28. Holzer, P. (1998). Neurogenic vasodilatation and plasma leakage in the skin. Gen. Pharmacol. *30*, 5–11. https://doi.org/10.1016/s0306-3623(97)00078-5.
29. Lasconi, C., Pifferi, S., Hernandez-Clavijo, A., Merigo, F., Cecchini, M.P., Gonzalez-Velandia, K.Y., Agostinelli, E., Sbarbati, A., and Menini, A. (2019). Bitter tastants and artificial sweeteners activate a subset of epithelial cells in acute tissue slices of the rat trachea. Sci. Rep. *9*, 8834. https://doi.org/10.1038/s41598-019-45456-w.
30. Barry, C.M., Ji, E., Sharma, H., Yap, P., Spencer, N.J., Matusica, D., and Haberberger, R.V. (2018). Peptidergic nerve fibers in the urethra: Morphological and neurochemical characteristics in female mice of reproductive age. Neurourol. Urodyn. *37*, 960–970. https://doi.org/10.1002/nau.23434.
31. Mesnage, B., Gaillard, S., Godin, A.G., Rodeau, J.L., Hammer, M., Von Engelhardt, J., Wiseman, P.W., De Koninck, Y., Schlichter, R., and Cordero-Erausquin, M. (2011). Morphological and functional characterization of cholinergic interneurons in the dorsal horn of the mouse spinal cord. J. Comp. Neurol. *519*, 3139–3158. https://doi.org/10.1002/cne.22668.
32. Kandel, C., Schmidt, P., Perniss, A., Keshavarz, M., Scholz, P., Osterloh, S., Althaus, M., Kummer, W., and Deckmann, K. (2018). ENaC in Cholinergic Brush Cells. Front. Cell Dev. Biol. *6*, 89. https://doi.org/10.3389/fcell.2018.00089.
33. Schmidt, P., Perniss, A., Bodenbenner-Tuerich, M., Wiegand, S., Briand, L., and Deckmann, K. (2024). Tas1R3 Dependent and Independent Recognition of Sugars in the Urethra and the Role of Tuft Cells in this Process. Adv. Biol. *8*, e2400117. https://doi.org/10.1002/adbi.202400117.
34. Qiao, S., Alasmi, S., Wyatt, A., Wartenberg, P., Wang, H., Candlish, M., Das, D., Aoki, M., Grünewald, R., Zhou, Z., et al. (2023). Intra-pituitary follicle-stimulating hormone signaling regulates hepatic lipid metabolism in mice. Nat. Commun. *14*, 1098. https://doi.org/10.1038/s41467-023-36681-z.
35. Abdel Wadood, N., Hollenhorst, M.I., Elhawy, M.I., Zhao, N., Englisch, C., Evers, S.B., Sabachvili, M., Maxeiner, S., Wyatt, A., Herr, C., et al. (2025). Tracheal tuft cells release ATP and link innate to adaptive immunity in pneumonia. Nat. Commun. *16*, 584. https://doi.org/10.1038/s41467-025-55936-5.
36. Billipp, T.E., Fung, C., Webeck, L.M., Sargent, D.B., Gologorsky, M.B., Chen, Z., McDaniel, M.M., Kasal, D.N., McGinty, J.W., Barrow, K.A., et al. (2024). Tuft cell-derived acetylcholine promotes epithelial chloride secretion and intestinal helminth clearance. Immunity *57*, 1243–1259.e8. https://doi.org/10.1016/j.immuni.2024.03.023.
37. Zhao, S., Ting, J.T., Atallah, H.E., Qiu, L., Tan, J., Gloss, B., Augustine, G.J., Deisseroth, K., Luo, M., Graybiel, A.M., and Feng, G. (2011). Cell type-specific channelrhodopsin-2 transgenic mice for optogenetic dissection of neural circuitry function. Nat. Methods *8*, 745–752. https://doi.org/10.1038/nmeth.1668.
38. Saqui-Salces, M., Keeley, T.M., Grosse, A.S., Qiao, X.T., El-Zaatari, M., Gumucio, D.L., Samuelson, L.C., and Merchant, J.L. (2011). Gastric tuft cells express DCLK1 and are expanded in hyperplasia. Histochem. Cell Biol. *136*, 191–204. https://doi.org/10.1007/s00418-011-0831-1.
39. Middelhoff, M., Westphalen, C.B., Hayakawa, Y., Yan, K.S., Gershon, M.D., Wang, T.C., and Quante, M. (2017). Dclk1-expressing tuft cells: critical modulators of the intestinal niche? Am. J. Physiol. Gastrointest. Liver Physiol. *313*, G285–G299. https://doi.org/10.1152/ajpgi.00073.2017.
40. Nandigama, R., Ibañez-Tallon, I., Lips, K.S., Schwantes, U., Kummer, W., and Bschleipfer, T. (2013). Expression of nicotinic acetylcholine receptor subunit mRNA in mouse bladder afferent neurons. Neuroscience *229*, 27–35. https://doi.org/10.1016/j.neuroscience.2012.10.059.
41. Howitt, M.R., Lavoie, S., Michaud, M., Blum, A.M., Tran, S.V., Weinstock, J.V., Gallini, C.A., Redding, K., Margolskee, R.F., Osborne, L.C., et al. (2016). Tuft cells, taste-chemosensory cells, orchestrate parasite type 2 immunity in the gut. Science *351*, 1329–1333. https://doi.org/10.1126/science.aaf1648.
42. Mao, D., Yasuda, R.P., Fan, H., Wolfe, B.B., and Kellar, K.J. (2006). Heterogeneity of nicotinic cholinergic receptors in rat superior cervical and nodose ganglia. Mol. Pharmacol. *70*, 1693–1699.
43. Bschleipfer, T., Nandigama, R., Moeller, S., Illig, C., Weidner, W., and Kummer, W. (2012). Bladder outlet obstruction influences mRNA expression of cholinergic receptors on sensory neurons in mice. Life Sci. *91*, 1077–1081. https://doi.org/10.1016/j.lfs.2012.05.007.
44. de Groat, W.C., and Yoshimura, N. (2006). Mechanisms underlying the recovery of lower urinary tract function following spinal cord injury. Prog. Brain Res. *152*, 59–84. https://doi.org/10.1016/S0079-6123(05)52005-3.
45. Birder, L.A. (2010). Urothelial signaling. Auton. Neurosci. *153*, 33–40. https://doi.org/10.1016/j.autneu.2009.07.005.
46. Birder, L.A. (2013). Nervous network for lower urinary tract function. Int. J. Urol. *20*, 4–12. https://doi.org/10.1111/j.1442-2042.2012.03210.x.
47. Holzer, P. (1988). Local effector functions of capsaicin-sensitive sensory nerve endings: involvement of tachykinins, calcitonin gene-related peptide and other neuropeptides. Neuroscience *24*, 739–768. https://doi.org/10.1016/0306-4522(88)90064-4.
48. Lembeck, F. (1953). [Central transmission of afferent impulses. III. Incidence and significance of the substance P in the dorsal roots of the spinal cord]. Naunyn-Schmiedebergs Arch. Exp. Pathol. Pharmakol. *219*, 197–213.
49. Abelli, L., Conte, B., Somma, V., Parlani, M., Geppetti, P., and Maggi, C.A. (1991). Mechanical irritation induces neurogenic inflammation in the rat urethra. J. Urol. *146*, 1624–1626.
50. Lundberg, J.M., Brodin, E., Hua, X., and Saria, A. (1984). Vascular permeability changes and smooth muscle contraction in relation to capsaicin-sensitive substance P afferents in the guinea-pig. Acta Physiol. Scand. *120*, 217–227. https://doi.org/10.1111/j.1748-1716.1984.tb00127.x.
51. Maggi, C.A., Santicioli, P., Abelli, L., Parlani, M., Capasso, M., Conte, B., Giuliani, S., and Meli, A. (1987). Regional differences in the effects of capsaicin and tachykinins on motor activity and vascular permeability of the rat lower urinary tract. Naunyn-Schmiedebergs Arch Pharmacol *335*, 636–645. https://doi.org/10.1007/BF00166980.
52. Pinter, E., and Szolcsanyi, J. (1988). Inflammatory and antiinflammatory effects of antidromic stimulation of dorsal roots in the rat. Agents Actions *25*, 240–242. https://doi.org/10.1007/BF01965023.
53. Shishido, S.N., Varahan, S., Yuan, K., Li, X., and Fleming, S.D. (2012). Humoral innate immune response and disease. Clin. Immunol. *144*, 142–158. https://doi.org/10.1016/j.clim.2012.06.002.
54. Foxman, B. (2014). Urinary tract infection syndromes: occurrence, recurrence, bacteriology, risk factors, and disease burden. Infect. Dis. Clin. North Am. *28*, 1–13. https://doi.org/10.1016/j.idc.2013.09.003.

55. McLellan, L.K., and Hunstad, D.A. (2016). Urinary Tract Infection: Pathogenesis and Outlook. Trends Mol. Med. *22*, 946–957. https://doi.org/10.1016/j.molmed.2016.09.003.

56. Wagenlehner, F.M.E., Weidner, W., Perletti, G., and Naber, K.G. (2010). Emerging drugs for bacterial urinary tract infections. Expert Opin. Emerg. Drugs *15*, 375–397. https://doi.org/10.1517/14728214.2010.500613.

57. Wagenlehner, F.M.E., Weidner, W., Pilatz, A., and Naber, K.G. (2014). Urinary tract infections and bacterial prostatitis in men. Curr. Opin. Infect. Dis. *27*, 97–101. https://doi.org/10.1097/QCO.0000000000000024.

58. Conte, B., Maggi, C.A., and Meli, A. (1989). Vesico-inhibitory responses and capsaicin-sensitive afferents in rats. Naunyn-Schmiedebergs Arch Pharmacol *339*, 178–183. https://doi.org/10.1007/BF00165141.

59. Yang, Z., Dolber, P.C., and Fraser, M.O. (2010). Differential vulnerabilities of urethral afferents in diabetes and discovery of a novel urethra-to-urethra reflex. Am. J. Physiol. Renal Physiol. *298*, F118–F124. https://doi.org/10.1152/ajprenal.00281.2009.

60. de Groat, W.C., Griffiths, D., and Yoshimura, N. (2015). Neural control of the lower urinary tract. Compr. Physiol. *5*, 327–396. https://doi.org/10.1002/cphy.c130056.

61. Jung, S.Y., Fraser, M.O., Ozawa, H., Yokoyama, O., Yoshiyama, M., De Groat, W.C., and Chancellor, M.B. (1999). Urethral afferent nerve activity affects the micturition reflex; implication for the relationship between stress incontinence and detrusor instability. J. Urol. *162*, 204–212. S0022-5347(05)68742-3.

62. Clapp, T.R., Medler, K.F., Damak, S., Margolskee, R.F., and Kinnamon, S. C. (2006). Mouse taste cells with G protein-coupled taste receptors lack voltage-gated calcium channels and SNAP-25. BMC Biol. *4*, 7. https://doi.org/10.1186/1741-7007-4-7.

63. Frahm, S., Slimak, M.A., Ferrarese, L., Santos-Torres, J., Antolin-Fontes, B., Auer, S., Filkin, S., Pons, S., Fontaine, J.F., Tsetlin, V., et al. (2011). Aversion to nicotine is regulated by the balanced activity of beta4 and alpha5 nicotinic receptor subunits in the medial habenula. Neuron *70*, 522–535. https://doi.org/10.1016/j.neuron.2011.04.013.

64. Andersson, K.E., Soler, R., and Füllhase, C. (2011). Rodent models for urodynamic investigation. Neurourol. Urodyn. *30*, 636–646. https://doi.org/10.1002/nau.21108.

65. Steinwall, O., and Klatzo, I. (1966). Selective vulnerability of the blood-brain barrier in chemically induced lesions. J. Neuropathol. Exp. Neurol. *25*, 542–559. https://doi.org/10.1097/00005072-196610000-00004.

66. Schneider, C.A., Rasband, W.S., and Eliceiri, K.W. (2012). NIH Image to ImageJ: 25 years of image analysis. Nat. Methods *9*, 671–675. https://doi.org/10.1038/nmeth.2089.

STAR★METHODS

KEY RESOURCES TABLE

REAGENT or RESOURCE	SOURCE	IDENTIFIER
Antibodies		
Rabbit anti-TRPM5; 1:8000	Kaske et al., 2007	N/A
Goat anti-CGRP; 1:8000	Biotrend	Biotrend Cat# BT17-2090-07, RRID:AB_2243858
Rabbit anti-CGRP; 1:20000	Peninsula	Peninsula Laboratories Cat# T-4032 RRID:AB_518147
Rat-*anti*-substance P; 1:400	Santa Cruz	Santa Cruz Biotechnology Cat# sc-21715, RRID:AB_628299
Sheep anti-DCAMKL1 1:400	R&D System	R and D Systems Cat# AF7138, RRID:AB_10973467
Chicken-*anti*-GFP (green fluorescent protein); 1:2000	Novus	Novus Cat# NB100-1614 RRID:AB_10001164
Donkey IgG anti-chicken IgY (H + L), FITC-conjugate; 1:800	Dianova	Jackson ImmunoResearch Labs Cat# 703-095-155, RRID:AB_2340356
Donkey-*anti*-sheep IgG conjugated to cyanine 3; 1:2000	Dianova	Jackson ImmunoResearch Labs Cat# 713-165-003, RRID:AB_2340727
Donkey anti-rabbit IgG, Cy3-conjugate; 1:2000	Merck Millipore	(Millipore Cat# AP182C, RRID:AB_92588)
Donkey IgG anti-rabbit IgG (H + L), Cy5-conjugate; 1:400	Dianova	Jackson ImmunoResearch Labs Cat# 711-175-152, RRID:AB_2340607
Donkey anti-goat IgG, Cy3-conjugate; 1:1600	Merck Millipore	Millipore Cat# AP180C, RRID:AB_92570
Donkey-*anti*-goat IgG conjugated to cyanine 5; 1:1400	Dianova	Jackson ImmunoResearch Labs Cat# 705-175-147, RRID:AB_2340415
Donkey-*anti*-rat IgG Cy3; 1:1000	Dianova	(Jackson ImmunoResearch Labs Cat# 712-165-150, RRID:AB_2340666)
Chemicals, peptides, and recombinant proteins		
Adenosine 5′-triphosphate di(tris) salt hydrate (ATP)	Sigma Aldrich	A9062 CAS-No: 102047-34-7
CP96345	Sigma Aldrich	CP96345 CAS-No: 132746-60-2
BIBN4096BS	Sigma Aldrich	SML2426 CAS-No: 204697-65-4
Mecamylamine	Sigma Aldrich	M9020 CAS-No: 826-39-1
Metamizol (Vetalgin 500 mg/mL)	MSD	CAS-No: 5907-38-0
Isofluran	Baxter	CAS No.: 26675-46-7
Evans Blue	Sigma Aldrich	E2129 CAS No.: 314-13-6
Atropine	Sigma Aldrich	A0257 CAS No.: 5908-99-6

(*Continued on next page*)

Continued

REAGENT or RESOURCE	SOURCE	IDENTIFIER
Fura-2-AM	Thermo Fisher	F1221 CAS No.: 108964-32-5
Capsaicin	Sigma Aldrich	211275 CAS-No: 404-86-4
Denatonium benzoate	Sigma Aldrich	D5765 CAS No.: 3734-33-6
4′,5-diamidino-2-phenylindole (DAPI)	Sigma Aldrich	D9542 CAS No.: 28718-90-3
Clozapine N-oxide (CNO)	Tocris	4936, CAS No.: 34233-69-7 batch no.: 16B/295845
Critical commercial assays		
SP ELISA Kit	ENZO Liefe Sciences	ADI-900-018
CGRP ELISA Kit	Wuxi Donglin Sci & Tech Development	DL-CGRP-Mu
Experimental models: Organisms/strains		
Mouse: C57BL/6JRj	Janvier Labs	RRID:IMSR_RJ:C57BL-6JRJ
Mouse: Tg(Trpm5-EGFP)#Sdmk (TRPM5-GFP)	Clapp et al., 2006	RRID:MGI:5617485
Mouse: B6.Cg-Tg(RP23-268L19-EGFP) 2Mik/J (ChAT-eGFP)	The Jackson Laboratory	Stock No: 007902 RRID:IMSR_JAX:007902
Mouse: B6.Cg-Tg(Chat-COP4*H134R/EYFP, Slc18a3)6Gfng/J (ChAT-ChR2-YFP)	The Jackson Laboratory	Stock No: 005848; RRID:IMSR_JAX:005848
Mouse: B6.129P2-Trpm5^{tm1Dgen}/J (TRPM5$^{-/-}$)	The Jackson Laboratory	Stock No: 005848; RRID:IMSR_JAX:005848
Mouse: Chrna3-eGFP	Frahm et al., 2011	RRID:MMRRC_000243-UNC
Mouse: Pou2f3^{tm1Abek} (Pou2f3$^{-/-}$)	Matsumoto et al., 2011	RRID:MGI:5140072
Mouse: Rosa26-NLSiRFP720-2A-Gq (eR26-DREADD) knock-in mice (DREADD-control)	Sen Qiao et al., 2023	N/A
Mouse: TRPM5-IRES-Cre (TRPM5-IC) x eR26-DREADD: TRPM5-IC/eR26-DREADD mice (Trpm5-DREADD)	Sen Qiao et al., 2023	N/A
Oligonucleotides		
Actb RT-PCR primer: 5′-CCATCATGAAGTGTGACGTTGA-3′, 5′-CATCGTACTCCTGCTTGCTGAT-3′	Perniss et al. 2020	N/A
Trpm5 RT-PCR primer: *5′-TATGGCTTGTGGCCTATGGT-3′*, 5′-ACCAGCAGGAGAATGACCAG-3′	Perniss et al. 2020	N/A
GFP RT-PCR primer: 5′-AAGTTCATCTGCACCACCG-3′, 5′-TCCTTGAAGAAGATGGTGCG-3′	This Paper	N/A
β-MG RT-PCR Primer: 5′-ATTCACCCCCACTGAGACTG-3′, 5′-GCTATTTCTTTCTGCGTGCAT	Keshavarz et al. 2018	N/A
Software and algorithms		
GraphPrism 7	GraphPad Software	https://www.graphpad.com/scientificsoftware/prism/GraphPad Prism (RRID:SCR_002798)
ElisaAnalysis.com software	Leading Technology Group	ElisaAnalysis.com
ImageJ 1.49	NIH	https://imagej.nih.gov/ij/ImageJ (RRID:SCR_003070)

(*Continued on next page*)

Continued

REAGENT or RESOURCE	SOURCE	IDENTIFIER
Tecan Infinite 200 PRO Multimode Microplate Reader	Tecan	Tecan (RRID:SCR_020543)
Biorender	Biorender	Biorender (RRID:SCR_018361)
ZEN 2010B SP1	Zeiss	ZEISS ZEN Microscopy Software (RRID:SCR_013672)
Prizmatix Pulser software	Prizmatix	https://www.prizmatix.com/software.htm
Arivis Vision4D software	Arivis	https://kb.arivis.com/RRID:SCR_018000
Other		
Fetal Bovine Serum	Thermo Fisher	26140079

EXPERIMENTAL MODEL AND STUDY PARTICIPANT DETAILS

Animals

Chat-eGFP (B6.Cg-Tg(RP23-268L19-EGFP)2Mik/J; Stock No. 007902; RRID:IMSR_JAX:007902), *Chat*-ChR2-YFP (B6.Cg-Tg(Chat-COP4*H134R/EYFP,Slc18a3)6Gfng/J; Stock No. 014546; RRID:MGI:4950538) and *Trpm5*$^{-/-}$ (B6.129P2-Trpm5tm1Dgen/J; Stock No: 005848; RRID:IMSR_JAX:005848) mice were obtained from Jackson Laboratory (Bar Habor, ME, USA). *Trpm5*$^{-/-}$ *were* back-crossed (at least six generations) on to the C57BL/6J background. *Trpm5*-eGFP (Tg(Trpm5-EGFP)#Sdmk) *Pou2f3*$^{-/-}$ (Pou2f3^{tm1Abek}; RRID:MGI:5140072) mice were provided by R. F. Margolskee.[62] Mice with eGFP driven by the nAChRα3-promoter (*Chrna3*-eGFP (Tg (Chrna3-EGFP)BZ135Gsat; RRID:MMRRC_000243-UNC) were provided by I. Ibanez-Tallon (MDC Molecular Medicine, Berlin, Germany).[63] C57BL/6J mice were obtained from Janvier Labs (Le Genest-Saint-Isle, France). *Rosa26-NLSiRFP720-2A-Gq* (eR26-DREADD) knock-in mice (DREADD-control) and *TRPM5-IRES-Cre* (TRPM5-IC) x *eR26-DREADD*: *TRPM5-IC/eR26-DREADD* mice (*Trpm5*-DREADD) were bred at the Saarland University.[34] This study was carried out in accordance with the recommendations of the European Communities Council Directive of 24th November 1986 (86/609/EEC). The protocol was approved by the local authorities (Regierungspräsidium Giessen; reference no. 516_M, 571_M, 572_M, 573_M, G 26/2016, G 12/2020; veterinary officer Marburg; Ex-1-2020, AK-1-2023, Ex-15-2024; animal welfare committees of Saarland University; VM2025-34). In total, 264 C57BL/6J (233 females, 31 males), 96 *Trpm5*$^{-/-}$ (71 females, 25 males), 14 *Chat*-eGFP (7 females, 7 males), 4 *Trpm5*-eGFP (2 females, 2 Males), 23 *Chrna3*-eGFP (15 females, 8 males), 38 *Chat*-ChR2-YFP (18 females, 20 males), 18 Pou2f3 (4 females, 14 males) and 32 DREADD (16 females, 16 males) mice were used mice were used. All animals were anesthetized using isoflurane inhalation and sacrificed by cervical dislocation and subsequent exsanguination. Mice older than 10 weeks were used throughout.

METHOD DETAILS

Immunofluorescence

Organs from *Chrna3*-eGFP (*n* = 15, *Chat*-eGFP (*n* = 14), *Chat*-ChR2-YFP (*n* = 8) and *Trpm5*-eGFP mice (*n* = 4) used for immunofluorescence were either freshly dissected and fixed by immersion in or perfused with Zamboni solution (2% paraformaldehyde/15% saturated picric acid; Merck, Darmstadt, Germany, in 0.1 M phosphate buffer, pH 7.4). Specimens were washed in 0.1 M phosphate buffer, incubated overnight in 18% sucrose (Carl Roth) in 0.1 M phosphate buffer, embedded in Tissue-Tek O.C.T. Compound (Sakura Finetek USA, Inc., USA), frozen in liquid nitrogen and sectioned at 10 μm on a Microm HM560 cryostat (Thermo Fischer Scientific). Cryosections were further processed by saturating unspecific protein binding sites for 1 h in 0.005 M phosphate buffer containing 10% horse serum (Sigma Aldrich), 0.5% Tween 20 (Sigma Aldrich), 0.1% bovine serum albumin (BSA; Sigma Aldrich). The combinations of primary antibodies to be tested were diluted in 0.005 M phosphate buffer and applied overnight at 4°C. Then, sections were rinsed repeatedly in 0.1 M phosphate buffer, covered with appropriate fluorophore-conjugated secondary antibodies for one hour at room temperature, rinsed, post-fixed with phosphate-buffered 4% paraformaldehyde and mounted in carbonate-buffered glycerol (pH 8.6) containing 1 μg/mL 4′,5-diamidino-2-phenylindole (DAPI; Sigma Aldrich). Antibody characteristics are given in the key resources table.

Specificity of secondary reagents was validated by omission of primary antibodies. Sections were evaluated by epifluorescence microscopy (Axioplan 2 or Leica DM6, Leica, Wetzlar, Germany), with a confocal laser scanning microscope (LSM 710, Zeiss, Oberkochen, Germany and Stellaris 5, Leica). Overlay images were created using ImageJ (RRID:SCR_003070) or microscope software. Each antibody combination was applied to at least 3 different samples.

For optically cleared whole-mount immunostainings of urethrae (*n* = 3 each strain; *Chat*-eGFP and *Chrna3*-eGFP), mice were transcardially perfused with buffered 4% paraformaldehyde and post-fixed in the same fixative for two additional hours, and tissue clearing was done as described previously.[13] In brief urethrae were incubated overnight in 4% acrylamide at 4°C, polymerized for 3 h at 37°C, cleared with 8% sodium dodecyl sulfate for 48 h, and subsequently incubated overnight in 10% horse serum, 0.5%

Tween 20, and 0.1% bovine serum in phosphate-buffered saline (1.06 mM KH_2PO_4, 155.2 mM NaCl, 2.9 mM Na_2HPO_4-$7H_2O$, Thermo Fischer Scientific, Waltham, MA, USA)) to block nonspecific binding sites. Primary antibodies were diluted in 0.005 M phosphate buffer and applied for 48 h at room temperature followed by 48 h of incubation with the secondary antibodies. The samples were mounted in HistoDenz (refractive index: 1.47) (Sigma-Aldrich) for evaluation by confocal laser scanning microscopy. Distance between nerve fibers and UTC was measured manually using microscope software (ZEN, Zeiss). 3D rendering of confocal z-stacks was done using a custom-made AI driven denoising and rendering algorithm in Arivis Vision4D software.

Assessment of neuropeptide release from explanted urethrae

The urethrae of 75 C57BL/6J mice (51 females, 24 males), 29 *Trpm5*$^{-/-}$mice (13 females, 16 males), 30 *Chat*-ChR2-YFP mice positive (n = 22, 10 females, 12 males) and negative (n = 8, 4 females, 4 males) for ChR2, 32 DREADD mice (16 females, 16 males) or 18 Pou2f3 (4 females, 14 males) were dissected, and cut longitudinally to expose the epithelium. In male animals, the urethra was divided into two parts (penile and membranous part), and each of them was used as an independent sample for subsequent release experiments. The two samples from one individual were allocated to different experimental groups, taking care of having an overall mix of penile and membranous samples within one experimental condition. Samples were transferred to a 24-well cell culture plate containing 500 μL Dulbecco's Modified Eagle Medium (DMEM, Thermo Fisher Scientific), washed with 500 μL Gibco PBS (PBS; pH 7.4; Thermo Fischer Scientific) and incubated for 10 min in 210 μL PBS. Subsequently, supernatants were taken as unstimulated PBS control and frozen in liquid nitrogen. Urethrae were then stimulated for an additional 10 min period in a 210 μL volume. Urethrae from *Chat*-ChR2-YFP were put in PBS and stimulated with or without blue light (456 nm, 10 min, 8 Hz, and 25-ms pulse) duration using a UHP-T-DI-LED source (Prizmatix), a transistor-transistor logic pulse train generator (S/*N* 7276, Prizmatix, Israel), and an LED controller (ultra high power LED current controller, Prizmatix) controlled by Prizmatix Pulser software. Urethrae from C57BL/6J and Trpm5$^{-/-}$ mice were stimulated with denatonium (denatonium benzoate, 5 mM in PBS, Sigma Aldrich), denatonium (5 mM) and mecamylamine (Mec, 20 μM, Sigma Aldrich; in PBS), denatonium (5 mM) and atropine (Atr, 10 μM, Sigma Aldrich; in PBS) or capsaicin (1 mM, Sigma Aldrich; in PBS with 10% EtOH). DREADD mice were stimulated with Clozapine N-oxide (CNO 60 μM; Cat. no.: 4936, batch no.: 16B/295845; Tocris, Bristol, UK)

In a prior experimental setup, the urethrae of 23 C57BL/6J (16 females, 7 males) and of 25 Trpm5$^{-/-}$mice (16 females, 9 males) were exposed only once to either PBS or denatonium (25 mM in PBS) for 10 min or both consecutively (Figures S6A–S6C). Subsequently, supernatants were taken and frozen in liquid nitrogen. The weights of the tissue samples were determined using a precision scale (Scaltec Instruments GmbH, Goettingen, Germany). SP or CGRP were assessed in supernatants by ELISA kits (SP: ADI-900-018; Enzo Life Sciences, Farmingdale, NY, USA; CGRP: DL-CGRP-Mu; Wuxi Donglin Sci & Tech Development, Wuxi, China) according to the manufacturer's instructions using an ELISA plate reader (Tecan Infinite 200) and ElisaAnalysis.com software (Leading Technology Group, Melbourne, Australia). Neuropeptide concentrations in the supernatants were calculated from a standard curve using 4 parameter logistic regression and related to weight of stimulated tissue. Detection range for SP was 9.76–10000 pg/mL. Detection range for CGRP was 15.625–1000 pg/mL.

Calcium imaging

For neuron isolation from *Chrna3*-eGFP mice (n = 5, 4 females, 1 male), lumbosacral dorsal root ganglia (DRG) were removed and transferred to Hanks' Balanced Salt Solution (HBSS, Thermo Fischer Scientific) with 2 mg/mL dispase (Roche, Basel, Switzerland) and 2 mg/mL collagenase A (Sigma Aldrich). Ganglia were dissociated using glass pipettes varying in size, and incubated for 60 min at 37°C. The dissociated neurons were washed with L-15 medium (Thermo Fischer Scientific) with added 10% fetal calf serum (Thermo Fischer Scientific) and 1% penicillin-streptomycin (Sigma Aldrich), seeded on 8 mm glass cover slips in L-15 medium coated with poly-L-lysine (Sigma Aldrich) and laminin (Thermo Fischer Scientific) overnight. Cells on cover slips were loaded for 30 min with Fura-2 a.m. (8 μM, Thermo Fischer Scientific) and cover slips were put into a Delta T dish (Bioptechs Inc., Butler, PA, USA). During experiments, cover slips were heated to 37°C and continuously rinsed with Lockes's solution (in mM: 136 NaCl, 5.6 KCl, 1.2 $MgCl_2$, 2.2 $CaCl_2$, 1.2 NaH_2PO_4, 14.3 $NaHCO_3$ and 10 mM glucose, 37°C, pH 7.4) gassed for 30 min with CO_2, (Carl Roth). Changes in the intracellular calcium concentration ($[Ca^{2+}]_i$), determined by ratiometric measurement of individual GFP positive cells, were recorded using a Leica DM5000 B microscope (Leica) with an X-Cite 200 DC fluorescence lamp (Excelitas Technologies, Waltham, MA, USA).

GFP positive cells were excited at wavelengths 360 and 380 nm and the ratio of the emissions (360/380) was recorded every second. Recordings were made in 3 cycles. Each recording cycle started with a baseline recording of 60 s. After 60 s, 500 μL of either Lockes's solution, denatonium benzoate (5 mM, 10 mM, 25 mM, in Lockes's solution), or nicotine (100 μM, in Lockes's solution, Sigma Aldrich) were added and another recording phase of 60 s followed. Between cycles, cells were superperfused with Lockes's solution for 2 min. Increases in $[Ca^{2+}]_i$ of 10% above baseline levels were considered as positive response.[1,32,33] Baseline level was defined as the mean of $[Ca^{2+}]_i$ in the 30 s period immediately prior to stimulation. Only GFP positive cells reacting to nicotine and/or denatonium benzoate were included. GFP-positive cells that responded neither to nicotine nor to denatonium were excluded. Each denatonium benzoate concentration was tested on multiple cells (5 mM: 19 cells; 10 mM: 23 cells; 25 mM: 12 cells) in 5 independent experiments.

RT-PCR

RNA was extracted from tongue and lumbosacral DRG taken from *Chrna3*-eGFP mice ($n = 3$), using RNeasy Mini Kit (Qiagen, Hilden, Germany). cDNA synthesis was performed as follows: 1 μL DNase I (Invitrogen) and 1 μL 10× DNase I reaction buffer (Invitrogen) were added to 8 μL RNA and incubated in a thermal cycler at 25°C for 15 min. Digestion was stopped by adding 1 μL of Ethylenediaminetetraacetic acid (EDTA, Invitrogen) and incubating at 65°C for 10 min. A master mix consisting of 1 μL 10 mM desoxy-nucleoside triphosphate (dNTP) mix (Qiagen), 1 μL Superscript III reverse transcriptase (Invitrogen), 4 μL 10× reverse transcriptase buffer (Invitrogen), 2 μL 0.1 M Dithiothreitol (DTT, Invitrogen), 0.5 μL oligo (dT) (Invitrogen), and 0.5 μL random hexamers (Invitrogen) was added to the samples and incubated in a thermal cycler for 50 min at 42°C and for 10 min at 70°C. Samples processed without reverse transcriptase and PCR preparations without cDNA (H_2O) served as negative controls. PCR was performed as follows: PCR preparation contained 1 μL of cDNA, 0.5 μL of each intron spanning primer pair (20 pM), 2 μL of CoralLoad PCR buffer (Qiagen), 4 μL of Q-Solution (Qiagen), 0.4 μL 10 mM dNTP mix, 0.1 μL HotStarTaq Plus DNA polymerase (Qiagen) and 12 μL RNase free water (Qiagen). Cycling conditions were as follows: 9 min at 95°C, followed by 37 cycles of 30 s at 95°C, 30 s at 60°C, 30 s at 72°C. Samples were then kept at 72°C for 10 min. PCR products were separated by electrophoresis on a Tris-acetate-EDTA agarose gel (1.5% agarose, 12 μL/L ethidiumbromid, Invitogen). Visualization and gel documentation were performed with Intas gel documentation system (Intas Science Imaging Instruments GmbH, Goettingen, Germany).

Primer sequences and amplicon sizes: *Trpm5* forward 5′-tatggcttgtggcctatggt-3′, *Trpm5* reverse 5′-accagcaggagaatgaccag-3′, 235 bp (Thermo Fisher Scientific), *β-actin* forward 5′-ccatcatgaagtgtgacgttga-3′, *β-actin* reverse 5′-catcgtactcctgcttgctgat-3′, 249 bp (Thermo Fisher Scientific).

Plasma extravasation

In these experiments 166 female C57BL/6J mice and 42 female *Trpm5*$^{-/-}$ mice were used. After pre-experimental analgesia (metamizole; 100 mg/kg p.o., MSD, Haar, Germany), mice were anesthetized by isoflurane (Baxter Deutschland GmbH, Unterschleissheim, Germany) inhalation. Evans blue solution (20 mg/mL in 0.9% NaCl solution at body temperature; 5 mL/kg body weight, Sigma Aldrich, St. Louis, MO, USA) was injected into the lateral tail vein. After 5 min, 50 μL of either control solution (PBS), or, as a stimulus, capsaicin (10 mM in PBS with 10% ethanol), or denatonium benzoate (25 mM in PBS) were applied via a PE 10 polyethylene catheter.[64] Atropine (10 μM) and mecamylamine (20 μM) were dissolved in the respective stimulation solution. CP96345 (NK1R antagonist, 10 mg/kg, Sigma Aldrich) and BIBN4096BS (calcitonin gene-related peptide receptor antagonist, 1 mg/kg, Sigma Aldrich) were injected intravenously in combination with Evans blue solution (20 mg/mL Evans blue; 10% dimethyl sulfoxide, Sigma Aldrich). After 15 min, mice were sacrificed, and urethra and bladder were harvested and processed for photometric measurement or histological evaluation.

For histological evaluation, urethrae were embedded in Tissue-Tek O.C.T. Compound (Sakura Finetek Germany GmbH, Staufen, Germany) and frozen in liquid nitrogen. Urethral cross sections of 10 μm thickness were mounted in carbonate-buffered glycerol at pH 8.6 (Carl Roth, Karlsruhe, Germany). All images of sections include entire dissected tissue and were evaluated by epifluorescence microscopy (Axioplan 2, Zeiss or Leica DM6, Leica). Evans blue emits a bright red fluorescence when excited with green light (excitation filter 525–560 nm).[65] All images were taken at identical magnification (20× objective lens) and exposure time (30 ms). Area of the urethral epithelium and fluorescence intensity (FI) per mm^2 urethral epithelium were determined using ImageJ (https://imagej.nih.gov/ij)[66] was used to determine the area of the urethral epithelium and the fluorescence intensity (FI) per mm^2 of urethral epithelium. For this purpose, a region of interest containing only the urethral epithelium was drawn on each section, excluding the remaining tissue and the lumen. FI (%) of epithelial layer was calculated relative to PBS control, therefore FI of PBS control were set at 100%. Each data point represents the mean fluorescence intensity of at least 10 randomly selected sections with a minimum 100 μm gap between them.

For photometric measurement of Evans blue concentration in tissue samples, whole dissected urethrae were weighed and then incubated in 500 μL formamide (Carl Roth) for 24 h at 55°C. Photometric analysis of supernatants was performed with a Tecan Infinite 200 plate reader (Tecan Trading AG, Männedorf, Germany) at 600 nm absorbance. Evans blue concentration was calculated relative to PBS control.

QUANTIFICATION AND STATISTICAL ANALYSIS

Statistical analysis was performed as noted in Figure legends using Prism 8 (GraphPad Software Inc., La Jolla, CA, USA). Data significantly deviated from normal distribution and, therefore, were analyzed by non-parametric tests. P-values ≤ 0.05 were regarded as statistically significant. All "n" values reflect biological replicates.